Chapter 8 Additional Far Detector Physics Opportunities

The deep underground location of LBNE's LArTPC far detector will expand the range of science opportunities it can pursue to potentially include observation of solar and other low-energy neutrinos, dark matter, magnetic monopoles and nucleon-antinucleon transitions.

8.1 Solar Neutrinos

In the early 20^{th} century, Arthur Stanley Eddington suggested that nuclear reactions of protons fuel energy production in the Sun. After the discovery of the neutron, Hans Bethe [1] proposed that the first stage of these nuclear reactions involves the weak interaction: a β decay of a proton into a neutron, a positron and a neutrino accompanied by the fusion of that neutron with another proton to form deuterium. This proton-proton (pp) reaction $p+p \rightarrow {}^{1}_{1}\text{H}+e^{+}+\nu_e$ is the origin of most solar neutrinos (called pp neutrinos). In 0.2% of the cases deuterium is produced by the corresponding three-body reaction $p+e^{-}+p \rightarrow {}^{1}_{1}\text{H}+\nu_e$ (called pep) which produces monoenergetic solar neutrinos at 1.4 MeV. The pp reaction is the starting point of a chain of nuclear reactions which converts four protons into a ${}^{4}_{2}\text{He}$ nucleus, two positrons and two neutrinos. This reaction chain, shown in Figure 8.1, produces 98% of the energy from the Sun. In addition to pp and pep, neutrinos are produced by the reactions ${}^{7}_{4}\text{Be}+e^{-} \rightarrow {}^{7}_{3}\text{Li}+\nu_e$ (^{7}Be neutrinos) and ${}^{3}_{2}\text{He}+p \rightarrow {}^{4}_{2}\text{He}+e^{+}+\nu_e$ (*hep* neutrinos) as well as the β decay ${}^{8}_{5}\text{B} \rightarrow {}^{8}_{4}\text{Be}+e^{+}+\nu_e \rightarrow {}^{4}_{2}\text{He}+{}^{4}_{2}\text{He}+e^{+}+\nu_e$ (^{8}B neutrinos). Carl-Friedrich von Weizsäcker [2] complemented the pp-chain with a cyclical reaction chain dubbed *CNO cycle* after the principal elements involved (shown in the top right illustration of Figure 8.1). Although theorized to be responsible for only 2% of energy production in the Sun, the CNO cycle plays the dominant role in the energy production of stars heavier than 1.3 solar masses.

The expected spectra of neutrinos from the pp reaction chain [3] are shown as solid curves in the bottom diagram of Figure 8.1. Neutrinos from the CNO cycle are shown as dashed blue curves.

The chief motivation of Raymond Davis to build his pioneering solar-neutrino detector in the Homestake mine was the experimental verification of stellar energy production by the observation of the neutrinos from these nuclear processes. While he succeeded in carrying out the first measurements of solar neutrinos — and shared the 2002 Nobel Prize in physics for the results — the measured flux [4] fell short of solar model calculations: the *solar-neutrino problem*. Data from the Super–Kamiokande (SK) and SNO [5,6] experiments eventually explained this mystery 30 years later as due to flavor transformation. However, intriguing questions in solar-neutrino physics remain. Some unknowns, such as the fraction of energy production via the CNO cycle in the Sun,

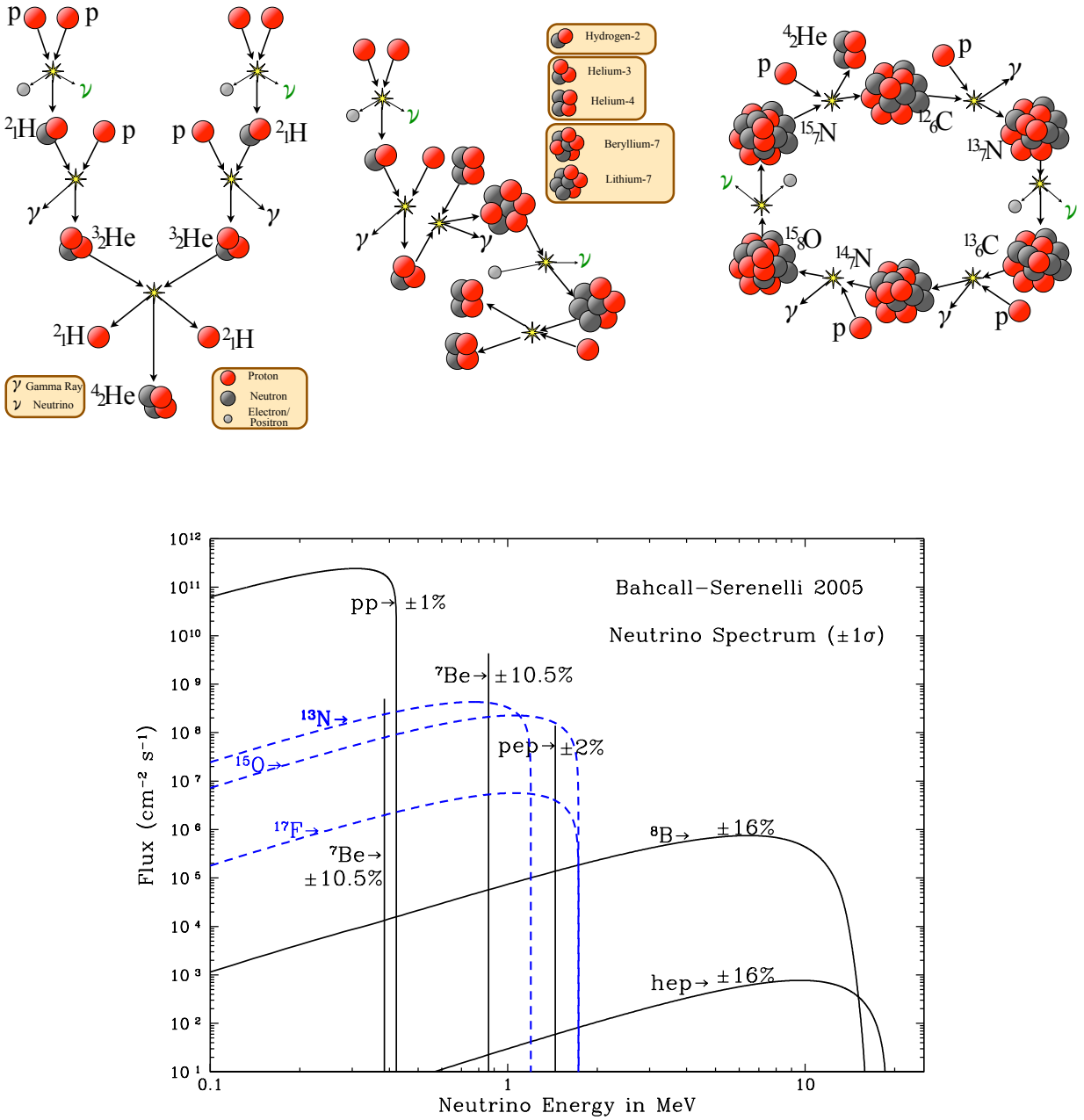

Figure 8.1: Top: the proton-proton and CNO reaction chain in the Sun. Bottom: solar-neutrino fluxes from [3].

flux variation due to helio-seismological modes that reach the solar core, or long-term stability of the solar core temperature, are astrophysical in nature. Others directly impact particle physics. Can the MSW model explain the amount of flavor transformation as a function of energy, or are nonstandard neutrino interactions required? Do solar neutrinos and reactor antineutrinos oscillate with the same parameters? Experimental data expected in the immediate future (e.g., further data

from Borexino [7] and SK as well as SNO+ [8]) will address some questions, but the high-statistics measurements necessary to further constrain alternatives to the standard oscillation scenario may need to wait for a more capable experiment such as LBNE.

Detection of solar and other low-energy neutrinos is challenging in a LArTPC because of high intrinsic detection energy thresholds for the charged-current (CC) interaction on argon (>5 MeV). To be competitive, this physics requires either a very low visible-energy threshold (∼1 MeV) or a very large mass (50 kt). However, compared with other technologies, a LArTPC offers a large cross section and unique signatures from de-excitation photons. Aggressive R&D efforts in low-energy triggering and control of background from radioactive elements may make detection in LBNE possible, and a large detector mass would make the pursuit of these measurements worthwhile.

The solar-neutrino physics potential of a large LArTPC depends primarily on its energy threshold and depth. The energy threshold is not only determined by the ability to pick up a low-energy electron, but also by the light collection of the photon-triggering system as well as background suppression. Only at a deep underground location will it have a reasonable chance of detecting solar neutrinos. In any detector of this kind, the decay of the naturally occurring ^{39}Ar produces β's with a 567-keV endpoint and an expected rate of 10 MHz per 10 kt of liquid argon. This limits the fundamental reach of LBNE to neutrino interactions with visible energies above 1 MeV. Possible signatures of solar neutrinos in LBNE are:

Elastic scattering of ^{8}B neutrinos with electrons: This signature would only reproduce the SK data; SK has already accumulated large statistics (>60,000 solar-neutrino events). An energy threshold of about 1 MeV (lower than the SK threshold which is currently 3.5 MeV [9]) would be required for a more interesting measurement of *pep* (defined in Figure 8.1) and CNO fluxes. Such solar-neutrino interactions are difficult to detect, as only low-energy single electrons (and neutrinos) are produced.

Charged-current interactions with argon: The signature for this interaction is:

$$\nu_e + {}^{40}\mathrm{Ar} \rightarrow {}^{40}\mathrm{K}^{*} + e^{-} \tag{8.1}$$

This signal is more interesting experimentally, as there is a signature of de-excitation photons and the visible energy is directly correlated with the neutrino energy; however, the reaction has an energy threshold of 5 MeV.

Cosmic-muon and fast-neutrino interactions with the ^{40}Ar nucleus (which are rather complex compared to interactions on ^{16}O or ^{12}C) are likely to generate many long-lived spallation products that could limit the detection threshold for low-energy neutrinos. Studies of the spallation background

in the LBNE LArTPC are underway. The production rate of ^{40}Cl, a beta emitter with an endpoint of 7.48 MeV that is a dominant source of background at energies above 5 MeV, is shown in Figure 8.2 as a function of depth. The cosmogenic background rates as a function of beta kinetic energy from several other beta emitters at the 4,850-ft level of Sanford Underground Research Facility are shown in Figure 6.8.

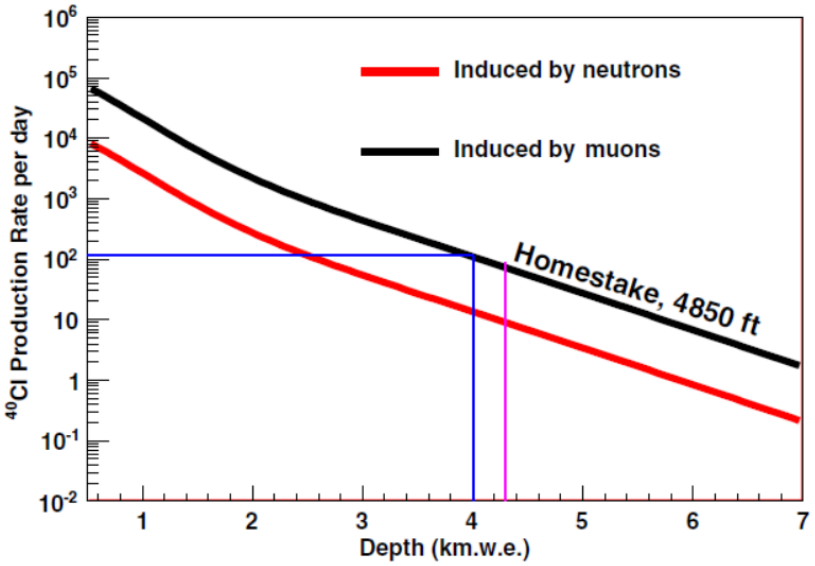

Figure 8.2: ^{40}Cl production rates in a 10-kt detector produced by (n,p) reaction as a function of depth.

In Table 8.1 the solar-neutrino event rate in a 34-kt LArTPC is shown, assuming a 4.5-MeV neutrino energy threshold and 31% ν_e.

Table 8.1: Solar-neutrino event rates in a 34-kt LArTPC assuming a 4.5-MeV neutrino energy threshold and an electron-flavor survival probability $P_{ee} = 31\%$.

Transition	Rate (evts/day)
Fermi	31
Gamow-Teller	88

The ICARUS Collaboration has reported a 10-MeV threshold [10]. Assuming the detector itself has low enough radioactivity levels, this threshold level would enable a large enough detector to measure the electron flavor component of the solar ^{8}B neutrino flux with high statistical accuracy. It could thereby further test the MSW flavor transformation curve (Figure 8.3) with higher statistical precision and potentially better energy resolution.

In addition to these solar matter effects, solar neutrinos also probe terrestrial matter effects with the variation of the ν_e flavor observed with solar zenith angle while the Sun is below the horizon — the *day/night effect*. A sizable effect is predicted only for the highest solar-neutrino energies, so while

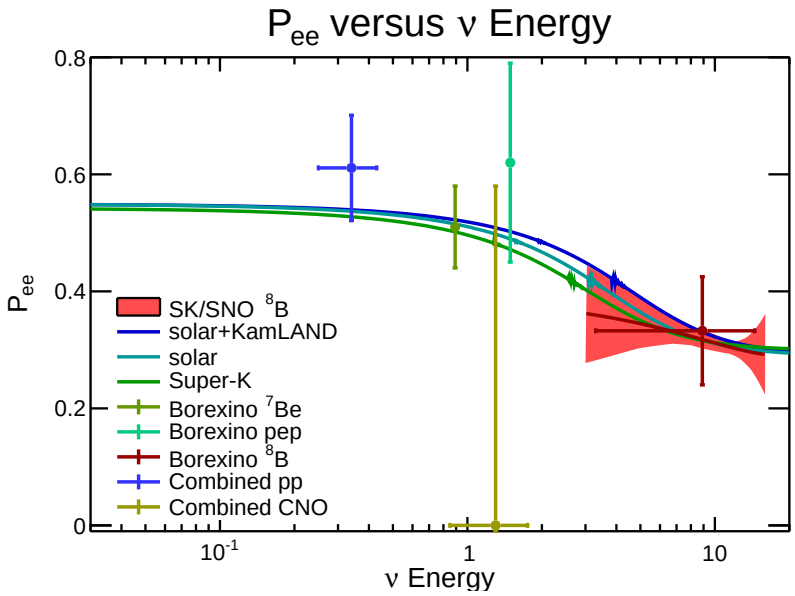

Figure 8.3: Measurements of the solar MSW transition. The red band combines SK and SNO ^{8}B data [11], the green measurements of ^{7}Be and pep are from Borexino [7,12] and the red error bar is Borexino's ^{8}B measurement [13]. The blue *pp* point and the yellow error bar (CNO) combine all solar data. MSW resonance curves for three different parameters are overlaid.

the comparatively high energy threshold is a handicap for testing the solar MSW resonance curve, it has a smaller impact on the high-statistics test of terrestrial matter effects. Recently, indication of the existence of the terrestrial matter effects were reported [14]. Measurements of this effect currently give the best constraints on the solar mass (Δm^2_{21}) splitting (Figure 8.4) using neutrinos rather than antineutrinos [15].

The comparison of ν disappearance to $\overline{\nu}$ disappearance tests CPT invariance. For good sensitivity to either solar-neutrino measurement, a liquid argon far detector of at least 34 kt is required.

8.2 Indirect Searches for WIMP Dark Matter

If the true nature of Dark Matter (DM) involves a weakly-interacting massive particle (WIMP) with a mass on the order of 1 GeV, an experiment could look for anomalous signals in astrophysical data from the annihilation (or decay) of DM into Standard Model particles, e.g., neutrinos [16]. Neutrinos produced by DM decay are expected to come from such distant objects as the galactic center, the center of the Sun or even from the Earth.

As our solar system moves through the DM halo, WIMPs interact with the nuclei of celestial bodies and become trapped in a body's gravitational well. Over time, the WIMPs accumulate near the core of the body, enhancing the possibility of annihilation. The high-energy neutrinos ($E \sim m_{\mathrm{WIMP}}$) from these annihilations can free-stream through the astrophysical body and emerge

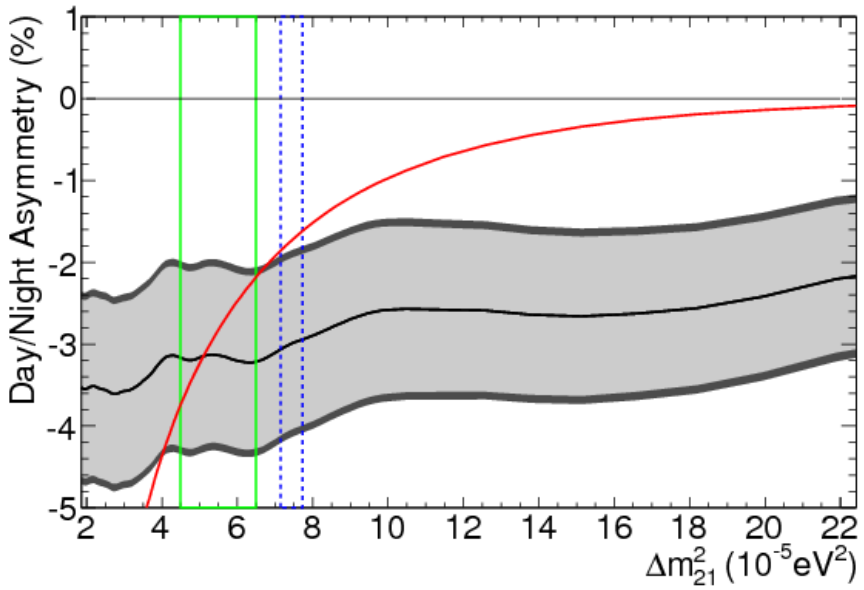

Figure 8.4: Dependence of the measured day/night asymmetry (fitted day/night amplitude times the expected day/night asymmetry in red) on Δm^2_{21}, for $\sin^2\theta_{12} = 0.314$ and $\sin^2\theta_{13} = 0.025$. The 1σ statistical uncertainties from the recent measurements by SK are given by the light grey band. The additional dark grey width to the band shows the inclusion of the systematic uncertainties. Overlaid are the 1σ allowed ranges from the solar global fit (solid green) and the KamLAND experiment (dashed blue). Figure is from [14].

roughly unaffected, although oscillation and matter effects can slightly alter the energy spectrum. Neutrinos produced via the nuclear-fusion processes in the Sun have energies close to 1 MeV, much lower than likely DM-decay neutrino energies.

The LBNE far detector's large mass and directional tracking capabilities will enable it to act as a *neutrino telescope* and search for neutrino signals produced by annihilations of dark matter particles in the Sun and/or the core of the Earth. Detection of high-energy neutrinos coming exclusively from the Sun's direction, for example, would provide clear evidence of dark matter annihilation [17].

IMB [18], IceCube [19] and SK, all water Cherenkov-based detectors, have searched for signals of DM annihilations coming from these sources, so far with negative results. A LArTPC can provide much better angular resolution than can water Cherenkov detectors, therefore providing better separation of the directional solar WIMP signal from the atmospheric-neutrino background. More thorough studies [20] are needed to determine whether LBNE could provide a competitive detection of dark matter.

8.3 Supernova Relic Neutrinos

Galactic supernovae are relatively rare, occurring somewhere between one and four times a century (Chapter 6). In the Universe at large, however, thousands of neutrino-producing explosions occur every hour. The resulting neutrinos — in fact most of the neutrinos emitted by all the supernovae since the onset of stellar formation — suffuse the Universe. Known both as *supernova relic neutrinos (SRN)* and as the *diffuse supernova-neutrino background (DSNB)*, their energies are in the few-to-30-MeV range. SRN have not yet been observed, but an observation would greatly enhance our understanding of supernova-neutrino emission and the overall core-collapse rate.

A liquid argon detector such as LBNE's far detector is sensitive to the ν_e component of the diffuse relic supernova-neutrino flux, whereas water Cherenkov and scintillator detectors are sensitive to the $\overline{\nu}_e$ component. However, backgrounds in liquid argon are as yet unknown, and a huge exposure ($>$500 kt $\cdot$ years) would likely be required for observation. Given a detector of the scale required to achieve these exposures (50 kt to 100 kt) together with tight control of backgrounds, LBNE — in the long term — could play a unique and complementary role in the physics of relic neutrinos.

In the current LBNE design, the irreducible background from solar neutrinos will limit the search for these relic neutrinos to an energy threshold greater than 18 MeV. Similarly, a search for relic antineutrinos is limited by the reactor-antineutrino background to a threshold greater than $\sim$10 MeV. The lower threshold and the smaller average ν_e energy relative to that for $\overline{\nu}_e$ (Figure 8.5) leads to the need for a larger detector mass.

A small but dedicated industry devotes itself to trying to predict the flux of these relic supernova neutrinos here on Earth [21,22,23,24,25,26,27,28]. Examples of two different predicted SRN spectra are shown in Figure 8.5, along with some of the key physics backgrounds from other neutrino sources.

In the LBNE LArTPC, relic supernova electron neutrinos would be detected primarily via the CC process as described by Equation 8.1. The electron track should be accompanied by evidence of ionization from the de-excitation of the potassium, e.g., shorter tracks sharing a common vertex; this is expected to help reduce backgrounds, but a detailed study has not yet been undertaken. In water Cherenkov and scintillator detectors, it is the $\overline{\nu}_e$ SRN flux that is detected through the process of inverse-beta decay. Unlike inverse-beta decay, for which the cross section is known to the several-percent level in the energy range of interest [29,30], the cross section for neutrino interactions on argon is uncertain at the 20% level [31,32,33]. Another limitation is that the solar *hep* neutrinos (defined in Figure 8.1), which have an endpoint at 18.8 MeV, will determine the lower bound of the SRN search window ($\sim$ 16 MeV). The upper bound is determined by the atmospheric ν_e flux as shown in Figure 8.5 and is around 40 MeV. Although the LArTPC provides a unique

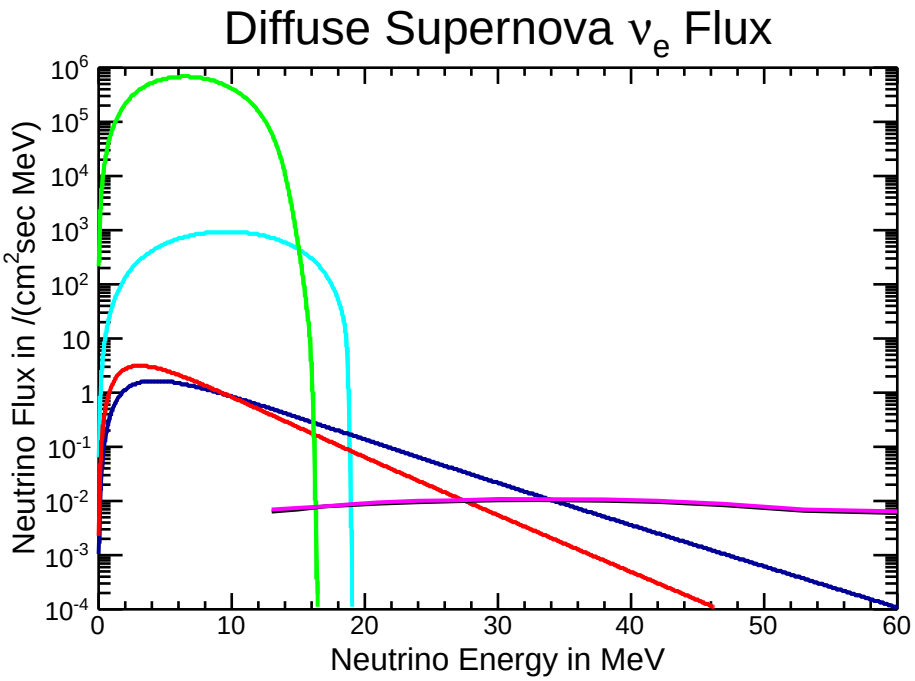

Figure 8.5: Predicted relic supernova ν_e spectra from two different models (red and blue) and some key neutrino backgrounds: ^{8}B solar ν_e (green), hep solar ν_e (cyan) and atmospheric ν_e (magenta).

sensitivity to the ν_e component of the SRN flux, early studies indicate that due to this lower bound of ∼16 MeV, LBNE would need a huge mass of liquid argon — of order 100 kt — to get more than 4σ evidence for the diffuse supernova flux in five years [34]. The expected number of relic supernova neutrinos, N_{SRN}, that could be observed in a 100-kt LArTPC detector in five years [34] assuming normal hierarchy is:

$$N_{\mathrm{SRN}} = 57 \pm 12, \quad 16\,\mathrm{MeV} \leq E_e \leq 40\,\mathrm{MeV}, \tag{8.2}$$

where E_e is the energy of the electron from the CC interaction as shown in Equation 8.1. The estimate of the SRN rate in Equation 8.2 has a weak dependence on the value of $\sin^2\theta_{13}$. The above calculation is valid for values of $\sin^2\theta_{13} > 10^{-3}$. The main challenge for detection of such a low rate of relic neutrinos in a LArTPC is understanding how much of the large spallation background from cosmic-ray interactions with the heavy argon nucleus (some of which are shown in Figure 6.8) leaks into the SRN search window.

8.4 GUT Monopoles

Searches for massive, slow-moving magnetic monopoles produced in the early Universe continue to be of pressing interest. Magnetic monopoles left over from the Big Bang are predicted by Grand Unified Theories, but to date have not been observed. Because of the very large masses set by the

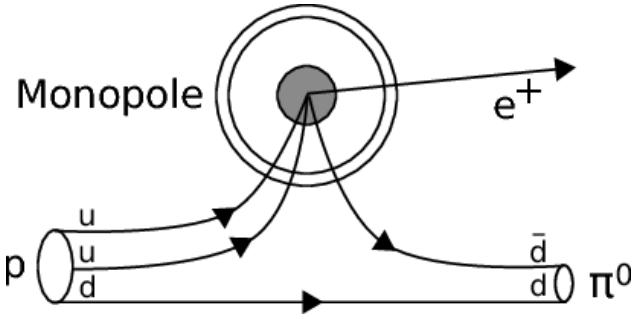

Figure 8.6: Illustration of a proton decay into a positron and a neutral pion catalyzed by a GUT monopole from [38].

GUT scale, these monopoles are normally non-relativistic, however searches for relativistic and ultra-relativistic monopoles are also of interest.

Relativistic monopoles are expected to be heavily ionizing, and hence best suited for detection in the large-area, neutrino-telescope Cherenkov detectors deployed in natural bodies of water or ice (e.g., [35,36]). With its much smaller active area, LBNE will most likely not be competitive in searches for fast monopoles.

Massive GUT monopoles are postulated to catalyze nucleon decay (Figure 8.6). It is possible that large underground detectors could detect this type of signal from transiting monopoles [37,38] via a signature consisting of multiple proton decays concurrent with the monopole's passage through the detector. Proton decay catalyzed by magnetic monopoles may be easier to observe in a LArTPC due to its superior imaging capability as compared to Cherenkov detectors, namely its high detection efficiency for a wider variety of proton decay modes, and its low energy thresholds. Whether these features are sufficient to overcome the limitation of smaller detector area relative to the very large neutrino telescopes has yet to be studied.

It should also be possible for LBNE to detect slow-moving monopoles via time-of-flight measurements, thereby eliminating reliance on the assumption of a proton-decay catalysis signature. The most stringent limits from direct searches for GUT monopoles with velocities in the range $4 \times 10^{-5} < \beta < 1$ have been obtained by the MACRO experiment [39], which has excluded fluxes at the level of $1.4 \times 10^{-16}\,\mathrm{cm^{-2}\,s^{-1}\,sr^{-1}}$. These limits probe the flux region just beyond that excluded by the existence of the galactic magnetic field (as characterized in variants of the Parker Bound).

The LBNE LArTPC far detector provides an opportunity to extend the reach of direct searches for slow monopoles, thanks to excellent timing and ionization measurement capabilities. Quantitative studies of sensitivity have yet to be carried out, but it is likely that the full-scope LBNE far detector will exceed the 10,000 m · sr isotropic-flux acceptance of MACRO.

8.5 Neutron-Antineutron Oscillations ($\Delta B = 2$)

Some Grand Unified Theories suggest the existence of double baryon-number-violating transitions that change nucleons into antinucleons [40]. The nucleon-antinucleon annihilation resulting from such a transition would provide an unmistakable signal in the LBNE LArTPC.

The imaging properties of the detector — superior to those of water detectors — would enable observation of nucleon annihilation final states in which the signal is broadened by the mix of charged and neutral hadrons. This signal could, however, be suppressed in a LArTPC if the neutron-to-antineutron transition rate is suppressed for bound neutrons due to interactions with the other nucleons.

8.6 Geo and Reactor $\overline{\nu}_e$'s

Electron antineutrinos ($\overline{\nu}_e$'s) produced by radioactive decays of the uranium, thorium and potassium present in the Earth are referred to as *geo-antineutrinos*. Decays of these three elements are currently understood to be the dominant source of the heat that causes mantle convection, the fundamental geological process that regulates the thermal evolution of the planet and shapes its surface. Detection of these geo-antineutrinos near the Earth's surface can provide direct information about the deep-Earth uranium and thorium content.

Geo-antineutrino energies are typically below 3.5 MeV. Reactor antineutrinos are somewhat more energetic, up to 8 MeV.

In a LArTPC, electron antineutrinos can in principle be detected by argon inverse-beta decay, represented by

$$\overline{\nu}_e + {}^{40}\mathrm{Ar} \rightarrow {}^{40}\mathrm{Cl}^* + e^+. \tag{8.3}$$

However, the threshold for this reaction is about 8.5 MeV, leading to the conclusion that an ^{40}Ar detector cannot use this method to detect either geo-antineutrinos or reactor antineutrinos.

Interaction via elastic scattering with electrons, another potential avenue, presents other obstacles. Not only are the recoil electrons from this interaction produced at very low energies, but solar neutrinos scatter off electrons and form an irreducible background roughly a thousand times larger than the geo-antineutrino signal. Although LBNE's location far away from any nuclear reactors leaves only a small reactor-antineutrino background and is thus favorable for geo-antineutrino detection, another detector technology (e.g., liquid scintillator) would be required to do so.

References

1. H. Bethe, "Energy production in stars," *Phys.Rev.* **55** (1939) 434–456. Cited in Section 8.1 (pg.195).
2. C. Weizsäcker, "Über Elementumwandlungen im Innern der Sterne II," *Physik.Z.* **39** (1938) 633–646. Cited in Section 8.1 (pg.195).
3. J. N. Bahcall, A. M. Serenelli, and S. Basu, "New solar opacities, abundances, helioseismology, and neutrino fluxes," *Astrophys.J.* **621** (2005) L85–L88, arXiv:astro-ph/0412440 [astro-ph]. Cited in Section 8.1 (pg.195).
4. B. Cleveland, T. Daily, R. Davis Jr., J. R. Distel, K. Lande, *et al.*, "Measurement of the solar electron neutrino flux with the Homestake chlorine detector," *Astrophys.J.* **496** (1998) 505–526. Cited in Section 8.1 (pg.195).
5. S. Fukuda *et al.*, **Super-Kamiokande Collaboration** , "Solar B-8 and hep neutrino measurements from 1258 days of Super-Kamiokande data," *Phys.Rev.Lett.* **86** (2001) 5651–5655, arXiv:hep-ex/0103032 [hep-ex]. Cited in Section 8.1 (pg.195).
6. Q. Ahmad *et al.*, **SNO Collaboration** , "Measurement of the rate of nu/e + d -> p + p + e- interactions produced by B-8 solar neutrinos at the Sudbury Neutrino Observatory," *Phys.Rev.Lett.* **87** (2001) 071301, arXiv:nucl-ex/0106015 [nucl-ex]. Cited in Section 8.1 (pg.195).
7. G. Bellini, J. Benziger, D. Bick, S. Bonetti, G. Bonfini, *et al.*, "Precision measurement of the 7Be solar neutrino interaction rate in Borexino," *Phys.Rev.Lett.* **107** (2011) 141302, arXiv:1104.1816 [hep-ex]. Cited in Section 8.1 (pg.197).
8. C. Kraus, **SNO+ Collaboration** , "SNO with liquid scintillator: SNO+," *Prog. Part. Nucl. Phys.* **57** (2006) 150–152. Cited in Section 8.1 (pg.197).
9. H. Sekiya, **Super-Kamiokande Collaboration** , "Solar neutrino analysis of Super-Kamiokande," arXiv:1307.3686, 2013. Cited in Section 8.1 (pg.197).
10. A. Guglielmi, **ICARUS Collaboration** , "Status and early events from ICARUS T600," *Nucl.Phys* **B (Proc. Suppl.) 229-232** (2012) 342–346. Cited in Section 8.1 (pg.198).
11. B. Aharmim *et al.*, **SNO Collaboration** , "Combined Analysis of all Three Phases of Solar Neutrino Data from the Sudbury Neutrino Observatory," *Phys.Rev.* **C88** (2013) 025501, arXiv:1109.0763 [nucl-ex].
12. G. Bellini *et al.*, **Borexino Collaboration** , "First evidence of pep solar neutrinos by direct detection in Borexino," *Phys.Rev.Lett.* **108** (2012) 051302, arXiv:1110.3230 [hep-ex].
13. G. Bellini *et al.*, **Borexino Collaboration** , "Measurement of the solar 8B neutrino rate with a liquid scintillator target and 3 MeV energy threshold in the Borexino detector," *Phys.Rev.* **D82** (2010) 033006, arXiv:0808.2868 [astro-ph].
14. A. Renshaw *et al.*, **Super-Kamiokande Collaboration** , "First Indication of Terrestrial Matter Effects on Solar Neutrino Oscillation," arXiv:1312.5176 [hep-ex], 2013. Cited in Section 8.1 (pg.199).

15. A. Gando *et al.*, **KamLAND Collaboration** , "Reactor On-Off Antineutrino Measurement with KamLAND," arXiv:1303.4667 [hep-ex], 2013. Cited in Section 8.1 (pg.199).
16. J. Silk, K. A. Olive, and M. Srednicki, "The Photino, the Sun and High-Energy Neutrinos," *Phys.Rev.Lett.* **55** (1985) 257–259. Cited in Section 8.2 (pg.199).
17. M. Cirelli, N. Fornengo, T. Montaruli, I. A. Sokalski, A. Strumia, *et al.*, "Spectra of neutrinos from dark matter annihilations," *Nucl.Phys.* **B727** (2005) 99–138, arXiv:hep-ph/0506298 [hep-ph]. Cited in Section 8.2 (pg.200).
18. J. LoSecco, J. Van der Velde, R. Bionta, G. Blewitt, C. Bratton, *et al.*, "Limits on the Flux of Energetic Neutrinos from the Sun," *Phys.Lett.* **B188** (1987) 388. Cited in Section 8.2 (pg.200).
19. M. Aartsen *et al.*, **IceCube Collaboration** , "Search for dark matter annihilations in the Sun with the 79-string IceCube detector," *Phys.Rev.Lett.* **110** (2013) 131302, arXiv:1212.4097 [astro-ph.HE]. Cited in Section 8.2 (pg.200).
20. M. Blennow, M. Carrigan, and E. F. Martinez, "Probing the Dark Matter mass and nature with neutrinos," *JCAP* **1306** (2013) 038, arXiv:1303.4530 [hep-ph]. Cited in Section 8.2 (pg.200).
21. T. Totani, K. Sato, and Y. Yoshii, "Spectrum of the supernova relic neutrino background and evolution of galaxies," *Astrophys.J.* **460** (1996) 303–312, arXiv:astro-ph/9509130 [astro-ph]. Cited in Section 8.3 (pg.201).
22. K. Sato, T. Totani, and Y. Yoshii, "Spectrum of the supernova relic neutrino background and evolution of galaxies," 1997. Cited in Section 8.3 (pg.201).
23. D. Hartmann and S. Woosley, "The cosmic supernova neutrino background," *Astropart.Phys.* **7** (1997) 137–146. Cited in Section 8.3 (pg.201).
24. R. Malaney, "Evolution of the cosmic gas and the relic supernova neutrino background," *Astropart.Phys.* **7** (1997) 125–136, arXiv:astro-ph/9612012 [astro-ph]. Cited in Section 8.3 (pg.201).
25. M. Kaplinghat, G. Steigman, and T. Walker, "The Supernova relic neutrino background," *Phys.Rev.* **D62** (2000) 043001, arXiv:astro-ph/9912391 [astro-ph]. Cited in Section 8.3 (pg.201).
26. S. Ando, J. F. Beacom, and H. Yuksel, "Detection of neutrinos from supernovae in nearby galaxies," *Phys.Rev.Lett.* **95** (2005) 171101, arXiv:astro-ph/0503321 [astro-ph]. Cited in Section 8.3 (pg.201).
27. C. Lunardini, "Testing neutrino spectra formation in collapsing stars with the diffuse supernova neutrino flux," *Phys.Rev.* **D75** (2007) 073022, arXiv:astro-ph/0612701 [astro-ph]. Cited in Section 8.3 (pg.201).
28. M. Fukugita and M. Kawasaki, "Constraints on the star formation rate from supernova relic neutrino observations," *Mon.Not.Roy.Astron.Soc.* **340** (2003) L7, arXiv:astro-ph/0204376 [astro-ph]. Cited in Section 8.3 (pg.201).
29. P. Vogel and J. F. Beacom, "Angular distribution of neutron inverse beta decay, anti-neutrino(e) + p —> e+ + n," *Phys.Rev.* **D60** (1999) 053003, arXiv:hep-ph/9903554 [hep-ph]. Cited in Section 8.3 (pg.201).

30. A. Strumia and F. Vissani, "Precise quasielastic neutrino nucleon cross section," *Phys. Lett.* **B564** (2003) 42–54, arXiv:astro-ph/0302055. Cited in Section 8.3 (pg.201).
31. W. E. Ormand, P. M. Pizzochero, P. F. Bortignon, and R. A. Broglia, "Neutrino capture cross-sections for Ar-40 and Beta decay of Ti-40," *Phys. Lett.* **B345** (1995) 343–350, arXiv:nucl-th/9405007. Cited in Section 8.3 (pg.201).
32. E. Kolbe, K. Langanke, G. Martinez-Pinedo, and P. Vogel, "Neutrino nucleus reactions and nuclear structure," *J. Phys.* **G29** (2003) 2569–2596, arXiv:nucl-th/0311022. Cited in Section 8.3 (pg.201).
33. M. Sajjad Athar and S. K. Singh, "nu/e (anti-nu/e) - Ar-40 absorption cross sections for supernova neutrinos," *Phys. Lett.* **B591** (2004) 69–75. Cited in Section 8.3 (pg.201).
34. A. Cocco, A. Ereditato, G. Fiorillo, G. Mangano, and V. Pettorino, "Supernova relic neutrinos in liquid argon detectors," *JCAP* **0412** (2004) 002, arXiv:hep-ph/0408031 [hep-ph]. Cited in Section 8.3 (pg.202).
35. R. Abbasi *et al.*, **IceCube Collaboration** , "Search for Relativistic Magnetic Monopoles with IceCube," *Phys.Rev.* **D87** (2013) 022001, arXiv:1208.4861 [astro-ph.HE]. Cited in Section 8.4 (pg.203).
36. M. Aartsen *et al.*, **IceCube Collaboration** , "The IceCube Neutrino Observatory Part IV: Searches for Dark Matter and Exotic Particles," arXiv:1309.7007 [astro-ph.HE], 2013. Cited in Section 8.4 (pg.203).
37. K. Ueno *et al.*, **Super-Kamiokande Collaboration** , "Search for GUT Monopoles at Super-Kamiokande," *Astropart.Phys.* **36** (2012) 131–136, arXiv:1203.0940 [hep-ex]. Cited in Section 8.4 (pg.203).
38. M. Aartsen *et al.*, **IceCube Collaboration** , "Search for non-relativistic Magnetic Monopoles with IceCube," arXiv:1402.3460 [astro-ph.CO], 2014. Cited in Section 8.4 (pg.203).
39. M. Ambrosio *et al.*, **MACRO Collaboration** , "Final results of magnetic monopole searches with the MACRO experiment," *Eur.Phys.J.* **C25** (2002) 511–522, arXiv:hep-ex/0207020 [hep-ex]. Cited in Section 8.4 (pg.203).
40. R. Mohapatra, "Neutron-Anti-Neutron Oscillation: Theory and Phenomenology," *J.Phys.* **G36** (2009) 104006, arXiv:0902.0834 [hep-ph]. Cited in Section 8.5 (pg.204).